

Tuning the Optical Property and Photocatalytic Performance of Titanate Nanotube toward Selective Oxidation of Alcohols under Ambient Conditions

Zi-Rong Tang,^{†,*} Yanhui Zhang,^{†,‡} and Yi-Jun Xu^{†,‡}

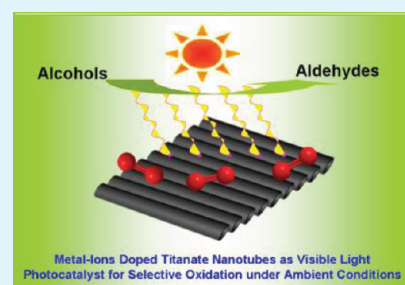
[†]College of Chemistry and Chemical Engineering, Fuzhou University, Fuzhou 350108, P.R. China

[‡]State Key Laboratory Breeding Base of Photocatalysis & College of Chemistry and Chemical Engineering, Fuzhou University, Fuzhou 350002, P.R. China

S Supporting Information

ABSTRACT: Titanate nanotube (TNT) represents one class of novel one-dimensional semiconducting nanomaterials that can be used as photocatalyst for given applications. However, TNT is only UV-light photoactive because of its intrinsic limitation of light absorption in the UV region. Here, we report a facile approach to tune the optical property and photocatalytic performance of TNT by doping various metal ions (Cu^{2+} , Co^{2+} , Ni^{2+} , Fe^{2+} , and Mn^{2+}) via an ion-exchange method in an aqueous phase. The optical properties of TNT can be finely tuned by incorporating different kinds of metal ions into its tubular framework. In particular, the incorporation of metal ions into the matrix of TNT is able to extend its light absorption to the visible-light region, thus making TNT have the visible-light photoactivity. Activity testing on photocatalytic selective oxidation of a variety of benzylic and allylic alcohols under mild conditions demonstrates that these metal-ion-doped TNTs exhibit markedly enhanced catalytic performance as compared to the undoped TNTs under both the irradiation of UV light and visible light. Such an enhancement of photocatalytic activity with regard to metal-ion-doped TNT is primarily attributed to the prolonged lifetime of photogenerated electron–hole pairs in comparison with that of undoped TNT. Our current research work demonstrates the tunable optical property of TNT by doping metal ions and, more significantly, opens promising prospects of one-dimensional nanotubular TNT or TNT-based materials as visible-light-driven photocatalyst in the area of selective transformation using molecular oxygen as benign oxidant under ambient conditions.

KEYWORDS: titanate nanotubes, metal-ions doping, visible light photocatalysis, selective oxidation, alcohols, ambient conditions



1. INTRODUCTION

One-dimensional semiconducting nanostructures, such as nanorods, nanowires, and nanotubes, play a key role in the current nanoscience and technology.^{1–6} Indeed, they have found potential applications in many fields, including photodetectors, light waveguides, solar energy conversion, lithium batteries, gas sensing, and photocatalysis.^{1–16} Titanium dioxide (TiO_2) is a well-known semiconductor photocatalyst that can be used for degradation of environmental pollutants, water splitting to hydrogen, and selective organic transformation.^{17–22} In particular, one-dimensional titanate nanotubes (TNT) have been remaining a subject of many investigations including studies of their physicochemical and crystallographic properties, their mechanism of formation, improving the method of synthesis and their applications.^{23–28} To date, the template method,^{29–31} anodic oxidation,^{32,33} and hydrothermal wet chemical treatment have been developed to synthesize TNT.^{34–38} In particular, the advantages of easy scale-up synthesis at low temperature and high yield make the preparation approach of hydrothermal treatment of TiO_2 particles with alkali solutions attract a lot of interest.^{15,34–38} So far, the potential applications based on TNT have been reported in numerous fields, ranging from heterogeneous catalysts, hydrogen storage materials, and secondary batteries.^{15,39–46}

Our primary interest focuses on the application of TNT in heterogeneous photocatalysis because of its novel chemical structure and electronic properties.^{15,39–42} In comparison to the commonly used nanoparticles or bulk materials, nanotubular TNT can provide unique benefits as photocatalyst in view of the following features.^{15,39–42,47–53} First, the one-dimensional geometry facilitates fast and long-distance electron transport. Second, nanotubular structure is expected to have large specific surface area and pore volume. Third, the light absorption and scattering can be markedly enhanced because of the high length-to-diameter ratio for one-dimensional nanotubular TNT. Therefore, it should be of significant interest to investigate the potential applications of such nanotubular TNT-based materials as photocatalysts for target applications. In fact, it has been reported that one-dimensional TNT can be used for “non-selective” degradation of organic pollutants, e.g., azo dyes and volatile organic pollutant.^{15,39–42,51–53} However, it should be noted that TNT is only UV-light photoactive because of its intrinsic limitation of light absorption in the UV region.^{15,39–42,51–53} Notably, one

Received: December 9, 2011

Accepted: February 27, 2012

Published: February 27, 2012

important structure feature for TNT is its high cation-exchange capacity.^{38,45,52} The residual sodium ions in TNT is not only able to stabilize the tubular framework structure^{15,38,45,52} but also provides the possibility of tuning the optical property by introducing different transition metal ions into the matrix of nanotubular TNT framework.^{38,52,54,55} As a result, the light absorption of TNT could be extended to the visible light region and, therefore, the photoactivity of TNT could also be finely tuned by doping different metal ions.

In addition, a literature survey leads us to find that the utilization of nanotubular TNT as photocatalyst for selective organic synthesis has not been reported so far. Besides the “non-selective” degradation of organic pollutants, synthesis of fine chemicals by photocatalytic selective redox process has shown the promising potential in the field of heterogeneous photocatalysis.^{22,56–59} By means of controlling the reaction conditions coupled with the choice of proper semiconductor photocatalysts, the high selectivity is able to be achieved for photocatalytic selective redox reactions. For example, it has been shown recently that graphene-TiO₂ nanocomposites can be used as visible-light-driven photocatalyst toward selective oxidation of alcohols to aldehydes,²² a key transformation for fine chemicals because carbonyl compounds such as aldehyde and ketone derivatives are widely utilized in the fragrance, confectionary, and pharmaceutical industries.^{56–59}

Herein, we report the modification of light absorption property of nanotubular TNT by a simple cation-exchange process with transition metal ions,^{38,45} including Fe²⁺, Co²⁺, Ni²⁺, Cu²⁺, and Mn²⁺, and their application as a visible-light photocatalyst in selective oxidation of alcohols using molecular oxygen as oxidant under ambient conditions. The introduction of transition metal ions is able to transform TNT into a visible-light-active photocatalyst. In addition, the doping of transition metal ions can improve the photocatalytic activity of TNT under the irradiation of UV light because of the improved lifetime of photogenerated electron–hole pairs. Our work demonstrates that the optical property of TNT can be tuned by doping metal ions, which extends its light absorption range to the visible light region. The introduction of metal ions into nanotubular framework of TNT is able to enhance its photocatalytic activity toward selective oxidation of alcohols under both the UV light and visible-light irradiation. One-dimensional nanotubular TNT-based materials has a promising potential as a visible-light-driven photocatalyst for selective transformation using molecular oxygen as benign oxidant under ambient conditions.

2. EXPERIMENTAL SECTION

2.1. Synthesis of Titanate Nanotube (TNT) and Metal-Ion-Doped TNT. The chemicals of NaOH, ethanol, ammonia solution, and metal-ions precursor of M(CH₃COO)₂ (M = Fe, Co, Ni, Cu, and Mn) were obtained from Sinopharm Chemical Reagent Co., Ltd. (Shanghai, China). Anatase titania nanosized powder (10 nm in size) was supplied from Alfa Aesar Co., Ltd. (Tianjin, China). All of the chemicals are analytic grades and used as received without further purification. Deionized water used in the synthesis was from local sources.

For the synthesis of TNT, anatase titania powder (0.5 g), and an aqueous solution of concentrated NaOH (10 M, 40 mL) were mixed and kept stirring to form a homogeneous suspension, which was then transferred into a Teflon-lined autoclave and hydrothermally treated at 140 °C for 12 h in an oven. After the reaction, the precipitate was separated by filtration and washed with deionized water until a pH value near 8 was reached. It should be mentioned that it is crucial for

the post-treatment of washing process with the control pH 8, which can help retain the intact tubular framework structure for further calcination at high temperature.¹⁵ The precipitate was then dispersed in anhydrous ethanol with the assist of ultrasonication. After a second filtration and washing step by ethanol, the sample was dried in a vacuum oven at 80 °C overnight. The sample is finally calcined at 400 °C for 6 h in air, which is denoted as TNT.

The synthesis of metal-ion-doped TNT is by an ion-exchange reaction of TNT with an aqueous ammonia solution with Fe²⁺, Co²⁺, Ni²⁺, Cu²⁺, and Mn²⁺, respectively, because of the stability of TNT in a basic solution and the stabilization of these substituting ions by complexation with ammonia.^{15,38,52} In a typical process, the metal-ion precursors of M(CH₃COO)₂ (M = Fe, Co, Ni, Cu, and Mn) were dissolved in water to form the corresponding M²⁺ solution (3 mM) followed by adding diluted ammonia solution (25%) drop by drop to form clear solutions at room temperature. Then, the TNT nanotubes (0.5 g) were dispersed evenly in the respective metal-ion solutions (50 mL) and stirred with speed of 100 rpm for 20 h at room temperature in order to allow a sufficient ion-exchange process. After that, the products were carefully washed with diluted ammonia (25%) and deionized water several times with the control pH 8, and to avoid physical adsorption of the substituting ions on the surface of the TNT nanotubes. The as-obtained samples are denoted as TNT-Fe, TNT-Co, TNT-Ni, TNT-Cu, and TNT-Mn, respectively.

2.2. Characterization. The phase composition of the samples was determined by the powder X-ray diffraction (XRD) on a Bruker D8 Advance X-ray diffractometer at 40 kV and 40 mA with Ni-filtered Cu K α radiation. The optical properties were analyzed by the UV–vis diffuse reflectance spectroscopy (DRS) using a UV–vis spectrophotometer (Cary-500, Varian Co.), in which BaSO₄ was used as the internal standard. The nitrogen adsorption–desorption isotherm was carried out using a Micromeritic-ASAP2020 equipment. The photoluminescence (PL) spectra were obtained using an Edinburgh Analytical Instrument PLS920 system. Transmission electron microscopy (TEM) images were obtained using a JEOL model JEM 2010 EX instrument at the accelerating voltage of 200 kV. The X-ray photoelectron spectra (XPS) analysis was performed on a Thermo Scientific ESCA Lab250 spectrometer using monochromatic Al K α radiation under vacuum at 2 \times 10^{−6} Pa, a hemispherical analyzer and sample stage with multiaxial adjustability to obtain the composition on the surface of catalysts. All binding energies were calibrated by the C 1s peak of the surface adventitious carbon at 284.6 eV.

Electron spin resonance (ESR) signal of the radicals spin-trapped by 5,5-dimethyl-1-pyrroline-N-oxide (DMPO) was recorded on a Bruker EPR A300 spectrometer. The sample (5 mg) was dispersed in the solvent benzotrifluoride (BTF, 0.5 mL). Then, 25 μ L DMPO/benzyl alcohol solution (1:10, v/v) was added and oscillated to achieve the well-blending suspension. The settings for the ESR spectrometer were as follows: center field = 3507 G, microwave frequency = 9.84 GHz and power = 6.36 mW.

Photoelectrochemical measurements were performed in a home-made three electrode quartz cells with a PAR VMP3Multi Potentiostat apparatus. Pt plate was used as counter and Ag/AgCl electrode used as reference electrodes, while the working electrode was prepared on fluoride-tin oxide (FTO) conductor glass. The sample powder (10 mg) was ultrasonicated in 1 mL of anhydrous ethanol to disperse it evenly to get slurry. The slurry was spreading onto FTO glass whose side part was previously protected using Scotch tape. The working electrode was dried overnight under ambient conditions. A copper wire was connected to the side part of the working electrode using a conductive tape. Uncoated parts of the electrode were isolated with epoxy resin. The electrolyte was 0.2 M aqueous Na₂SO₄ solution (pH 6.8) without additive. The photoelectrochemical impedance spectroscopy experiments were taken on a CHI660D workstation.

2.3. Photocatalytic Activity. The photocatalytic selective oxidation of various alcohols was performed as the following.^{22,57–59} Typically, a mixture of alcohol (0.1 mmol) and 8 mg catalyst was dissolved in the solvent of benzotrifluoride (BTF) (1.5 mL), which was saturated with pure molecular oxygen from gas cylinder. The choice of solvent BTF is because of its inertness to oxidation and high

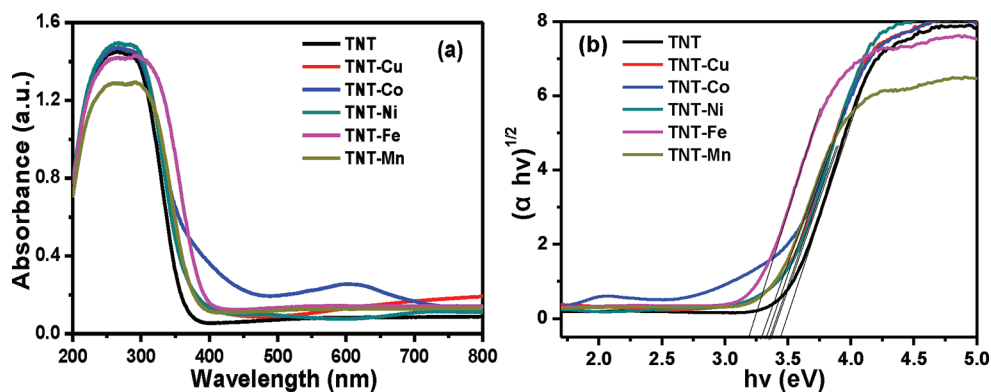


Figure 1. UV-vis diffuse reflectance spectra (DRS) of (a) undoped titanate nanotube (TNT) and various metal-ion-doped TNT, and (b) the plot of transformed Kubelka–Munk function versus the energy of light.

solubility for molecular oxygen.^{57–59} The above mixture was transferred into a 10 mL Pyrex glass bottle filled with molecular oxygen at a pressure of 0.1 MPa,^{22,57–59} and stirred for half an hour to make the catalyst blend evenly in the solution. For photocatalytic reaction under visible light irradiation, the suspensions were irradiated by a 300 W Xe arc lamp (PLS-SXE 300, Beijing Perfectlight Co. Ltd.) with a UV-CUT filter to cut off light of wavelength <420 nm. For photocatalytic reaction under UV light irradiation, the suspensions were irradiated by the same 300 W Xe arc lamp with a UV band-pass filter (365 ± 15 nm). After the reaction, the mixture was centrifuged at 12,000 rpm for 20 min to completely remove the catalyst particles. The remaining solution was analyzed with an Agilent Gas Chromatograph (GC-7820, with Capillary FFAP analysis column). The assignment of products was confirmed by a Hewlett-Packard Gas Chromatograph/Mass Spectrometry (HP-5973GC/MS). Conversion of alcohol, yield of aldehyde and selectivity for aldehyde were defined as the follows^{57–59}

$$\text{conversion (\%)} = [(C_0 - C_{\text{alcohol}})/C_0] \times 100 \quad (1)$$

$$\text{yield (\%)} = C_{\text{aldehyde}}/C_0 \times 100 \quad (2)$$

$$\text{selectivity (\%)} = [C_{\text{aldehyde}}/(C_0 - C_{\text{alcohol}})] \times 100 \quad (3)$$

where C_0 is the initial concentration of alcohol, C_{alcohol} and C_{aldehyde} are the concentration of the substrate alcohol and the corresponding aldehyde, respectively, at a certain time after the photocatalytic reaction.^{57–59}

3. RESULTS AND DISCUSSION

Figure S1 (Supporting Information) shows the typical sample photographs of pristine undoped titanate nanotube (TNT) and metal-ion-doped TNT. It can be seen that the introduction of metal ion into the matrix of TNT can lead to the color change of as-obtained samples, particularly for TNT-Cu, TNT-Co, and TNT-Ni. The optical property measurement of these samples, using the UV-vis diffuse reflectance spectra (DRS) as shown in Figure 1a, further evidence that the property of light absorption of TNT can be finely tuned by the introduction of different metal ions. In particular, the incorporation of metal ions into the framework of TNT is able to extend its light absorption to the visible-light region. Thus, metal-ion-doped TNT can be photoexcited by the irradiation of visible light and would presumably exhibit the visible light photocatalytic performance of TNT for target reactions. A plot obtained via the transformation based on the Kubelka–Munk function versus the energy of light is shown in Figure 1b, by which the roughly estimated band gap values are 3.43, 3.36, 3.32, 3.36, 3.18, and 3.28 eV corresponding to TNT, TNT-Cu, TNT-Co, TNT-Ni, TNT-Fe, and TNT-Mn, respectively. This indicates a band gap

narrowing of metal-ions doped TNT as compared to undoped TNT, which could be attributed to the formation of impurity energy levels of doped metal ions between the valence band and conduction band of TNT.

To confirm that the nanotubular framework structure is retained intact for metal-ion-doped TNT as compared with undoped TNT, we performed the powder X-ray diffraction (XRD) analysis.^{15,38,45} As displayed in Figure 2, the diffraction

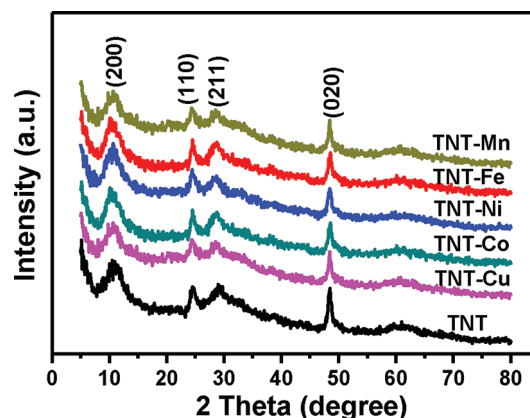


Figure 2. XRD patterns of undoped TNT and various metal-ion-doped TNT.

peaks at 2θ values of 10.7, 24.5, 29.2, and 48.5° can be indexed to (200), (110), (211), and (020) crystal planes of TNT phase, respectively.^{15,42,52} These main diffraction peaks are typical of layered titanates, especially the strong broad one around $2\theta = 10.7^\circ$, being attributed to the interlayer distance.^{42,52} All of the characteristic crystalline phase peaks of TNT have been maintained with regard to metal-ions doped TNT including TNT-Cu, TNT-Co, TNT-Ni, TNT-Fe, and TNT-Mn, clearly suggesting that the nanotubular structure of TNT is not collapsed.^{15,38,40–42,52} The transmission electron microscopy (TEM) analysis of these samples is in faithful agreement with the XRD results. That is, the nanotubular structure of TNT is maintained intact after the doping of metal ions into the matrix of TNT, as reflected by the TEM images in Figure 3. The average inner diameter of undoped and metal-ions doped TNT is ca. 5 nm, and the length is in the range of 80–500 nm.

The measured specific Brunauer–Emmett–Teller (BET) surface areas as shown in Figure S2 in the Supporting Information are ca. 379, 377, 380, 381, 378, and 381 m²/g, corresponding to

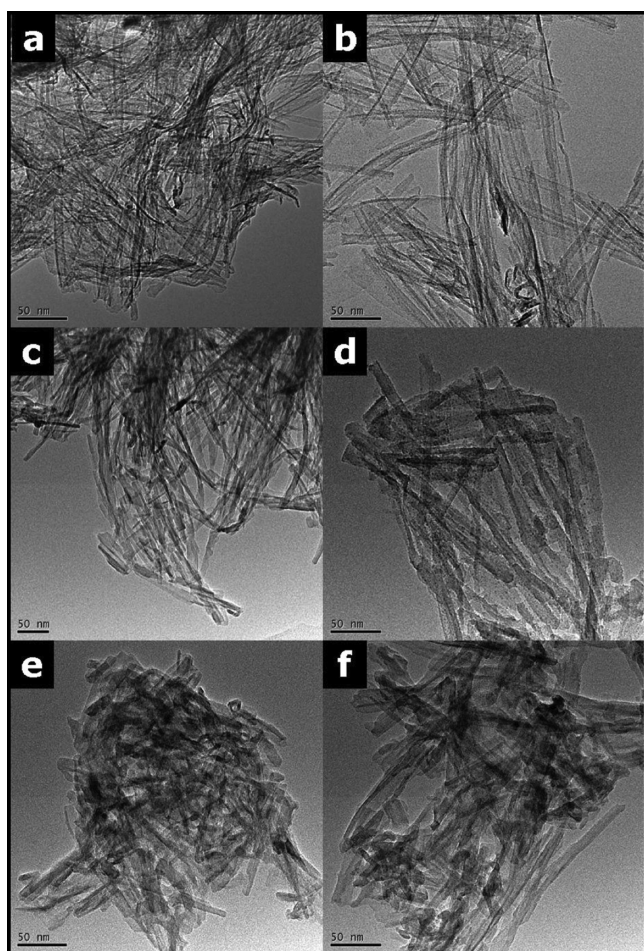


Figure 3. Typical TEM images of (a) undoped TNT, and various metal-ion-doped (b) TNT-Cu, (c) TNT-Co, (d) TNT-Ni, (e) TNT-Fe, and (f) TNT-Mn.

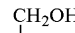
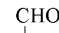
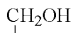
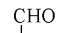
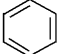
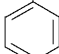
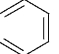
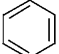
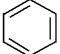
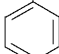
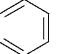
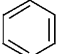
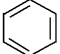
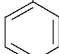
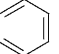
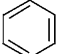
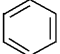
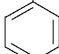
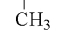
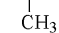
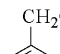
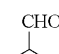
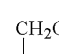
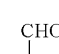
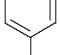

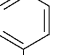
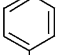
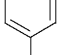

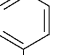
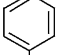
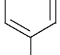

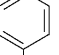
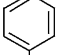
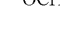
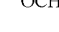
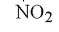
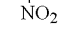
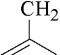
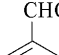
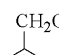
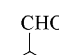
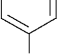
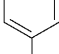
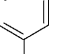
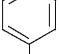
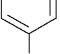
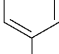
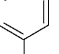
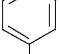
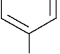
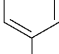
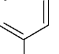
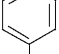
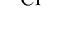

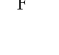

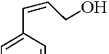
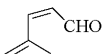
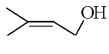
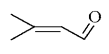
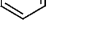
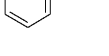


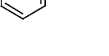
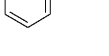


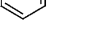
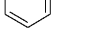


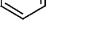
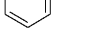


undoped TNT, doped TNT-Cu, TNT-Co, TNT-Ni, TNT-Fe, and TNT-Mn, respectively. In addition, they also have the similar total pore volumes and pore size distribution, as shown in Figure S2 in the Supporting Information. Therefore, the joint data of BET, XRD and TEM suggest that the doping of metal-ions plays a negligible effect on the nanotubular microstructure of TNT. The X-ray photoelectron spectra (XPS) analysis in Figure S3 in the Supporting Information shows that, as expected, the valence state of doped metal ions on the surface of all of the samples is $+2$.^{61–65} In particular, the peaks located at ca. 932.5 and 952.2 eV are attributed to Cu^{2+} . The peaks located at ca. 780.4 and 796.3 eV are attributed to Co^{2+} . The peaks located at ca. 855.4 and 872.6 eV are attributed to Ni^{2+} . The peaks located at ca. 709.2 and 722.8 eV are attributed to Fe^{2+} . The peaks located at ca. 640.6 and 652.3 eV are attributed to Fe^{2+} . On the basis of the quantification of XPS data, the doping contents of Cu^{2+} , Co^{2+} , Ni^{2+} , Fe^{2+} , and Mn^{2+} in the samples of metal-ion-doped TNT are calculated to be about 0.50, 0.51, 0.49, 0.50, and 0.49 mol %, respectively.

Tables 1 and 2 display the photocatalytic activity of selective oxidation of various alcohols, including benzylic alcohols and allylic alcohols, over the samples of undoped TNT and metal-ions doped TNT after the visible-light irradiation of 4 and 10 h, respectively, at room temperature and atmospheric pressure. It can be seen that all of the metal-ions doped TNTs exhibit visible light photoactivity toward selective oxidation of alcohols to aldehydes with high selectivity, ca. 90–100%. In contrast, the

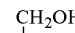
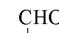
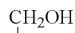
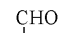
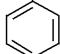
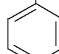
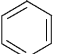
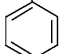


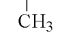
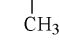
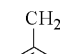
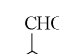
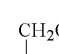
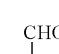
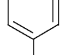
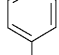
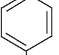
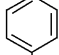




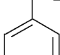
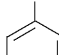
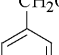
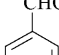
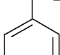
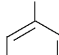
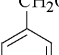
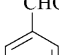
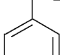
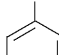
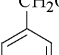
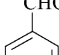
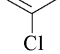
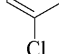
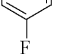
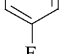




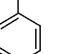
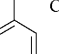
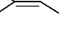
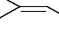
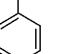
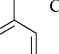
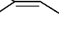
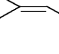
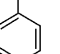
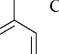
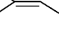
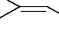






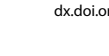
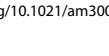
















undoped TNT shows very poor visible light photoactivity, as reflected by the very low conversion of alcohols, which is reasonable because the intrinsic limitation of visible light absorption for the undoped TNT.^{15,39–42,51–53} Increasing the irradiation time is able to enhance the conversion of alcohols over the photocatalyst of metal-ions doped TNT; however, the selectivity to corresponding aldehydes will be decreased moderately, as shown in Table 2. This observation is understandable in view of deep oxidation of target product of aldehydes after the longer reaction time. For example, regarding selective oxidation of benzyl alcohol over the photocatalyst of TNT-Mn, the conversion is ca. 13% along with ca. 100% selectivity to benzaldehyde after the visible light irradiation of 4 h. After the longer irradiation time of 10 h, the conversion is increased to 24% along with 98% selectivity. Blank experiments in the absence of catalysts and/or light show that no conversion of alcohols is observed, hence confirming the reaction is really driven by a photocatalytic process. Controlled experiment in the presence of nitrogen atmosphere shows trace conversion of alcohols, proving that molecular oxygen is the primary oxidant that selectively oxofunctionalizes substrate alcohols to corresponding aldehydes. In addition, it should be mentioned that the UV light photoactivity of TNT can also be improved significantly due to the doping of metal ions, as evidenced by Tables S1 and S2 in the Supporting Information. Therefore, the introduction of metal ions into the nanotubular framework of TNT is not only able to transform the only UV-light-active undoped TNT photocatalyst into the visible-light-active one but also markedly enhance the photoactivity of TNT under UV-light irradiation.

To understand why the doping of metal ions into the framework of TNT is able to improve its photocatalytic performance significantly, we have performed the photoelectrochemical experiments with regard to all of the samples, which can be used to reflect the lifetime of electron–hole pairs for photocatalysts upon light irradiation.^{22,58} Figure 4 shows the photocurrent transient response for the samples of undoped TNT and various metal-ion-doped TNT electrodes, under both UV light and visible-light irradiation, respectively. It can be seen that the doping of metal-ions into the tubular framework of TNT is able to remarkably enhance the photocurrent density upon both visible light and UV-light irradiation. These suggest that the lifetime of photogenerated electron–hole pairs can be markedly improved due to the doping of various metal ions, which well-account for the much higher photocatalytic activity of metal-ion-doped TNT than undoped TNT toward oxidation of alcohols to corresponding aldehydes. This prolonged lifetime of photogenerated charge carriers can also be confirmed by the photoluminescence (PL) spectra. As shown in Figure 5, the PL intensity obtained over metal-ions doped TNT is much weaker than that of undoped TNT, suggesting the longer lifetime of photogenerated electron–hole pairs. In addition, we have also done the photoelectrochemical impedance spectra, which is shown in Figure S4 in the Supporting Information. It is observed that, for metal-ions doped TNT, the semicircle in the plot becomes shorter, indicating a decrease in the solid state interface layer resistance and the charge transfer resistance on the surface.⁵⁸ Therefore, the PL spectra and photoelectrochemical analysis together demonstrate that the doping of metal ions is able to inhibit the recombination of photogenerated electron–hole pairs upon UV and visible-light irradiation. In addition, as mentioned above, the doping of metal ions plays a negligible effect on the surface area and pore volume of TNT,

Table 1. Selective Oxidation of a Range of Alcohols over the TNT and Metal-Ion-Doped TNT Photocatalysts under the Irradiation of Visible Light for 4 h

Catalyst	Substrate	Product	Conv. ^a (%)	Sel. ^a (%)	Substrate	Product	Conv. ^a (%)	Sel. ^a (%)
TNT			1.0	100			1.1	99
TNT-Cu			6.8	100			8.7	98
TNT-Co			7.5	100			8.5	98
TNT-Ni			8.2	100			8.7	98
TNT-Fe			4.9	100			9.9	98
TNT-Mn			13.0	100			10.9	99
TNT			1.2	98			1.0	98
TNT-Cu			8.1	98			7.6	98
TNT-Co			8.0	99			7.1	97
TNT-Ni			6.9	98			8.0	97
TNT-Fe			8.2	97			6.9	97
TNT-Mn			10.2	98			9.7	97
TNT			0.6	97			1.1	92
TNT-Cu			4.5	97			7.9	94
TNT-Co			4.7	96			7.9	93
TNT-Ni			4.6	96			8.2	92
TNT-Fe			5.0	97			7.6	93
TNT-Mn			5.7	96			11.2	92
TNT			0.7	91			0.3	90
TNT-Cu			5.5	93			3.6	91
TNT-Co			4.9	93			3.5	93
TNT-Ni			5.1	92			4.0	93
TNT-Fe			6.2	93			4.0	92
TNT-Mn			5.0	92			4.4	93

^athe standard deviation is <2%.**Table 2. Selective Oxidation of a Range of Alcohols over the TNT and Metal-Ion-Doped TNT Photocatalysts under the Irradiation of Visible Light for 10 h**

Catalyst	Substrate	Product	Conv. ^a (%)	Sel. ^a (%)	Substrate	Product	Conv. ^a (%)	Sel. ^a (%)
TNT			1.5	99			1.6	98
TNT-Cu			13.0	99			16.0	98
TNT-Co			15.0	99			16.0	98
TNT-Ni			16.0	99			16.0	98
TNT-Fe			10.0	99			18.0	98
TNT-Mn			24.0	98			20.0	98
TNT			1.7	98			1.3	97
TNT-Cu			16.0	98			15.0	97
TNT-Co			16.0	98			14.0	97
TNT-Ni			14.0	98			16.0	97
TNT-Fe			17.0	97			14.0	97
TNT-Mn			20.0	98			20.0	97
TNT			0.9	96			1.5	91
TNT-Cu			9.0	96			15.0	91
TNT-Co			8.0	96			16.0	91
TNT-Ni			8.0	96			16.0	91
TNT-Fe			10.0	96			15.0	91
TNT-Mn			10.0	96			20.0	89
TNT			1.0	88			0.7	86
TNT-Cu			9.0	89			7.0	87
TNT-Co			8.0	88			7.0	86
TNT-Ni			9.0	89			7.0	87
TNT-Fe			11.0	88			8.0	86
TNT-Mn			9.0	92			8.0	86

^aThe standard deviation is <2%.

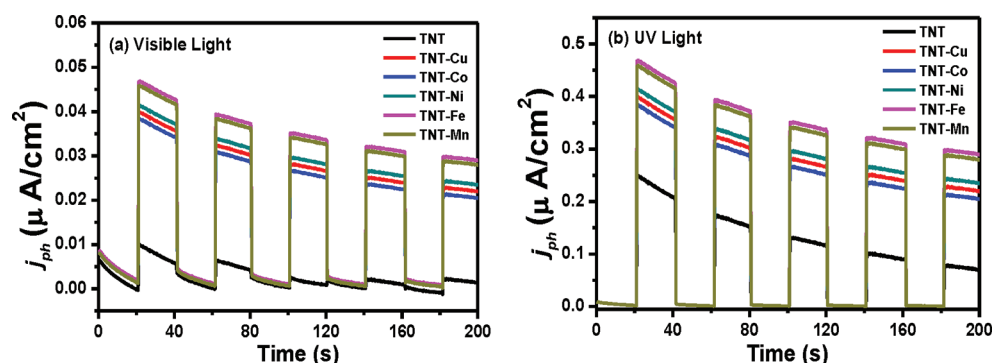


Figure 4. Photocurrent transient response of undoped TNT and metal-ions doped TNT in a 0.2 M of Na_2SO_4 aqueous solution under (a) visible light and (b) UV light irradiation, respectively.

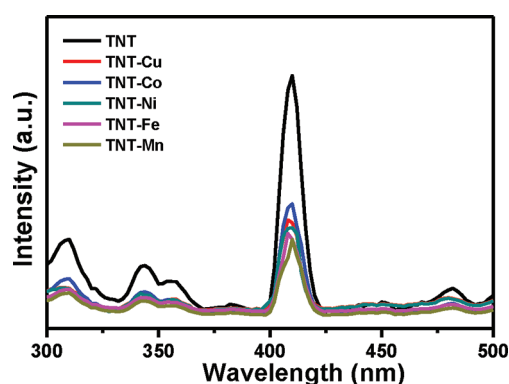


Figure 5. Photoluminescence (PL) spectra of undoped TNT and metal-ion-doped TNT.

which is in agreement with the adsorption data for undoped TNT and metal-ion-doped TNT toward alcohols in the dark as shown in Figure S5 in the Supporting Information. Thus, these two factors, i.e., surface area and pore volume, are not the primary reasons leading to the significant photoactivity difference between the undoped TNT and metal-ion-doped TNT toward selective oxidation of alcohols.

The electron spin resonance (ESR) analysis can render further evidence to support the fact that the doping of metal ions is able to promote the separation of photogenerated electron–hole pairs under both UV light and visible light irradiation. It has been well-known that, in photocatalytic process, molecular oxygen is an excellent electron acceptor regardless of nonselective photocatalytic degradation or selective photocatalytic transformation reaction.⁶⁰ Therefore, in principle, the so-called superoxide radical species ($\text{O}_2^{\cdot-}$) should be detected in the reaction system.^{22,57–59} If the lifetime of charge carriers, i.e., photogenerated electron–hole pairs, is lengthened for metal-ions doped TNT in comparison with the undoped TNT, the higher intensity of $\text{O}_2^{\cdot-}$ should be observed by the ESR analysis. Figure 6 shows the ESR spectra of $\text{O}_2^{\cdot-}$ trapped by 5,5-dimethyl-1-pyrroline-N-oxide (DMPO) for all of the samples under visible-light irradiation. It is obvious that the $\text{O}_2^{\cdot-}$ radical species can be observed for all of metal-ion-doped TNT whereas no apparent $\text{O}_2^{\cdot-}$ radical species are detected for the undoped TNT. This is in agreement with their optical absorption property and photoactivity as discussed above. In other words, because the undoped TNT does not have light absorption in the visible-light region, it is not able to effectively produce the electron–hole pairs upon visible-light irradiation. On the contrary, after the doping of metal ions, the light absorption range of TNT is extended to the

visible light region, thereby causing the visible light photoactivity for metal-ion-doped TNT. See Figure S6 in the Supporting Information shows the ESR spectra of $\text{O}_2^{\cdot-}$ trapped by DMPO for the undoped TNT and metal-ion-doped TNT under UV light irradiation. As can be seen, for all of the samples including undoped TNT and metal-ion-doped TNT, the $\text{O}_2^{\cdot-}$ radical species can be observed and their intensity is much stronger than that under visible light irradiation. This is in accordance with the higher photoactivity under the UV light irradiation than that under the visible light irradiation. A tentative mechanism for photocatalytic selective oxidation of alcohols to corresponding aldehydes over metal-ion-doped TNT can be proposed as the following, which is schematically displayed in Figure 7. Upon the visible-light irradiation, the doped metal ions as impurity energy levels can promote the visible light absorption and the generation of the photoexcited electron–hole pairs over the surface of metal-ion-doped TNT. The adsorbed alcohol on the metal-ion-doped TNT surface can be oxidized by the positive hole to give rise to alcohol radical cation,^{57,58} which reacts with molecular oxygen or superoxide radicals to produce the target product, corresponding aldehyde.

On the basis of above results, it can be concluded that the lifetime of photogenerated charge carriers is the most important factor that determines the overall photoactivity performance of the undoped TNT and metal-ions doped TNT upon UV light or visible-light irradiation toward selective oxidation of alcohols. Doping of metal ions into the framework of TNT is able to enhance the lifetime of photogenerated electron–hole pairs, thereby leading to the improved photoactivity of metal-ions doped TNT as compared to that of the undoped TNT. In addition, in view of the tunable optical property of TNT by facile substitution of a wide range of transition-metal ions via ion-exchange with sodium ions and proton ions in TNT,^{38,45,55} there would be a wide, promising potential to further optimize the photocatalytic performance of TNT and transform it into a visible-light active photocatalyst toward selective redox reactions.

4. CONCLUDING REMARKS

In summary, one-dimensional titanate nanotube (TNT) doped with various metal ions (Cu^{2+} , Co^{2+} , Ni^{2+} , Fe^{2+} , and Mn^{2+}) has been synthesized by an ion-exchange method in an aqueous phase. The optical properties of TNT are finely tuned by incorporating different kinds of metal ions. In particular, the incorporation of metal ions into the matrix of TNT is able to extend its light absorption to the visible-light region, thus making TNT exhibit the visible-light photoactivity toward selective oxidation of alcohols. These metal-ion-doped TNT samples

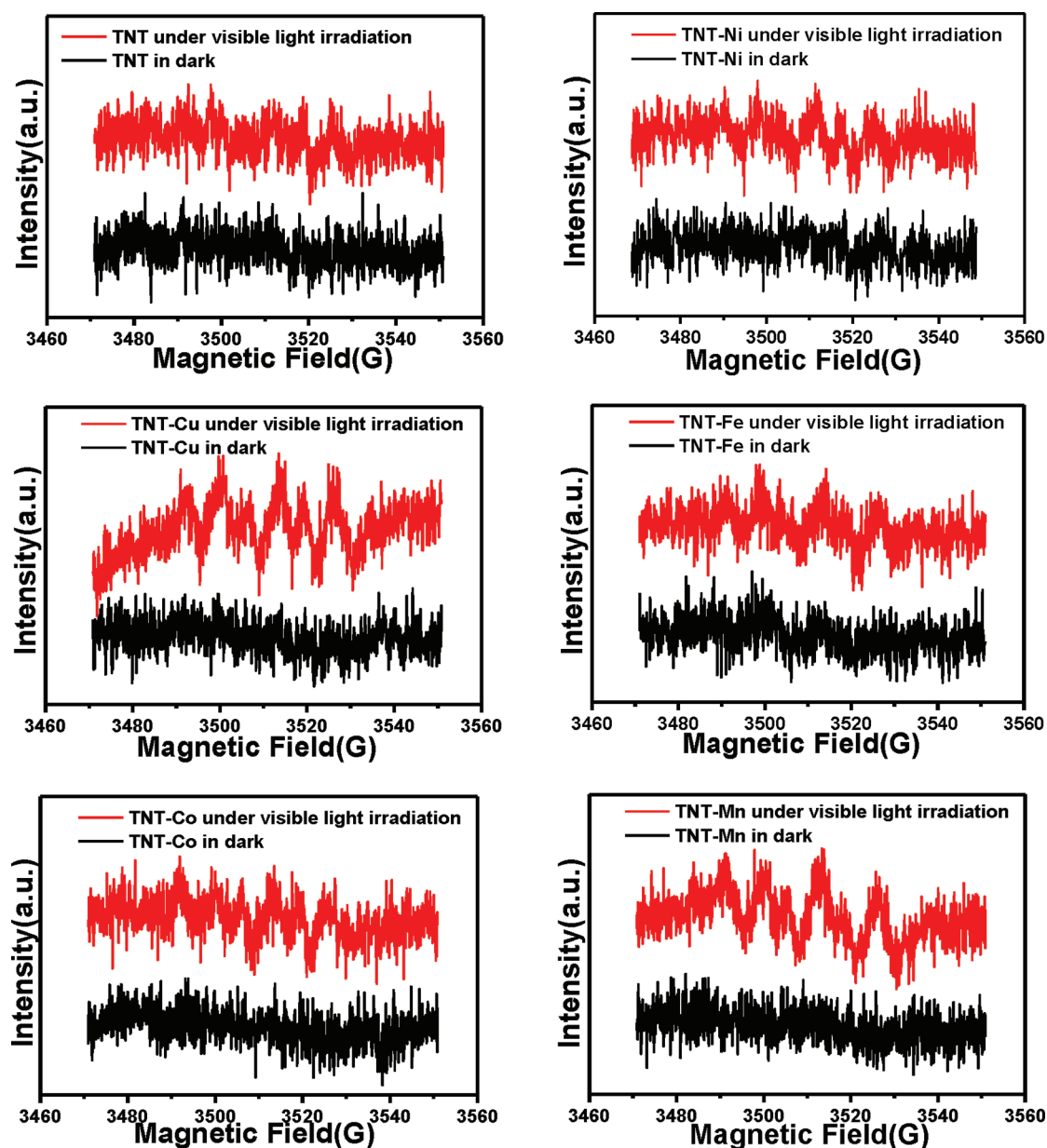


Figure 6. ESR spectra of superoxide radical adducts trapped by DMPO for the samples of undoped TNT and various metal-ion-doped TNT under visible light irradiation.

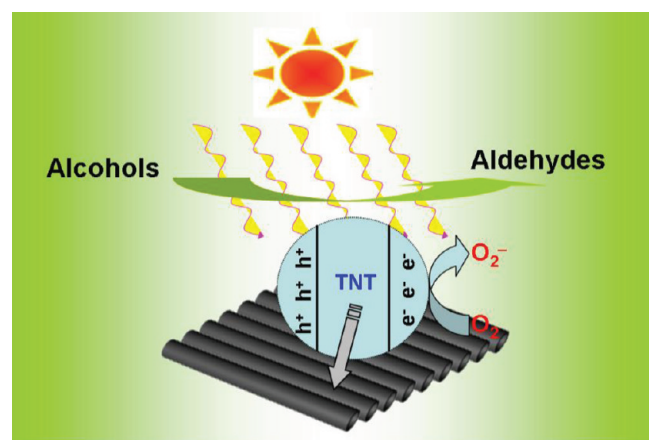


Figure 7. Proposed tentative mechanism for photocatalytic selective oxidation of alcohols to corresponding aldehydes over the metal-ion-doped TNT photocatalyst.

exhibit markedly enhanced catalytic performance toward selective oxidation of a range of benzylic and allylic alcohols as compared to the undoped TNT under both the irradiation of both UV light and visible light. This enhancement of photoactivity is primarily ascribed to the prolonged lifetime of photogenerated charge carriers for metal-ion-doped TNT in comparison with that of undoped TNT. Our work clearly demonstrates the tunable optical property of TNT by doping metal ions and, significantly, opens a new doorway of one-dimensional nanotubular TNT and other semiconductor nanotubes as a new type of visible-light-driven photocatalyst in selective transformation under ambient conditions.

■ ASSOCIATED CONTENT

Supporting Information

The photographs of undoped and metal-ions doped TNT samples, N_2 adsorption–desorption isotherms, X-ray photoelectron spectra (XPS), photoactivity data under the UV light

irradiation, Nyquist impedance plots under both the UV and visible light irradiation, the adsorption capacity of samples in the dark, and electron spin resonance (ESR) data under the UV light irradiation. This material is available free of charge via the Internet at <http://pubs.acs.org>.

AUTHOR INFORMATION

Corresponding Author

*Tel./fax: +86 591 22866126. E-mail: zrtang@fzu.edu.cn.

Notes

The authors declare no competing financial interest.

ACKNOWLEDGMENTS

The support by the National Natural Science Foundation of China (20903022, 20903023), the Award Program for Minjiang Scholar Professorship, Program for Changjiang Scholars and Innovative Research Team in Universities (PCSIRT0818), National Basic Research Program of China (973 Program: 2007CB613306), the Science and Technology Development of Foundation of Fuzhou University (2009-XQ-10), the Open Fund of Photocatalysis of Fuzhou University (0380038004), and Program for Returned High-Level Overseas Chinese Scholars of Fujian province is gratefully acknowledged.

REFERENCES

- (1) Rao, C. N. R.; Govindaraj, A. *Adv. Mater.* **2009**, *21*, 4208–4233.
- (2) Hochbaum, A. I.; Chen, R.; Delgado, R. D.; Liang, W.; Garnett, E. C.; Najarian, M.; Majumdar, A.; Yang, P. *Nature* **2008**, *451*, 163–167.
- (3) Huynh, W. U.; Dittmer, J. J.; Alivisatos, A. P. *Science* **2002**, *295*, 2425–2427.
- (4) Wu, D.; Liu, J.; Zhao, X.; Li, A.; Chen, Y.; Ming, N. *Chem. Mater.* **2006**, *18*, 547–553.
- (5) Tian, B.; Zheng, X.; Kempa, T. J.; Fang, Y.; Yu, N.; Yu, G.; Huang, J.; Lieber, C. M. *Nature* **2007**, *449*, 885–889.
- (6) Gautam, U. K.; Fang, X.; Bando, Y.; Zhan, J.; Golberg, D. *ACS Nano* **2008**, *2*, 1015–1021.
- (7) Chen, X.; Mao, S. S. *Chem. Rev.* **2007**, *107*, 2891–2959.
- (8) McPhillips, J.; Murphy, A.; Jonsson, M. P.; Hendren, W. R.; Atkinson, R.; Hook, F.; Zayats, A. V.; Pollard, R. J. *ACS Nano* **2010**, *4*, 2210–2216.
- (9) Wang, J.; Gudiksen, M. S.; Duan, X.; Cui, Y.; Lieber, C. M. *Science* **2001**, *293*, 1455–1457.
- (10) Mor, G. K.; Varghese, O. K.; Paulose, M.; Shankar, K.; Grimes, C. A. *Sol. Energy Mater. Sol. Cells* **2006**, *90*, 2011–2075.
- (11) Wang, Z. L. *ACS Nano* **2008**, *2*, 1987–1992.
- (12) Wang, Y.; Jiang, X.; Xia, Y. J. *Am. Chem. Soc.* **2003**, *125*, 16176–16177.
- (13) Zhai, T.; Fang, X.; Liao, M.; Xu, X.; Zeng, H.; Yoshio, B.; Golberg, D. *Sensors* **2009**, *9*, 6504–6529.
- (14) Tang, Z. R.; Zhang, Y.; Xu, Y. J. *RSC Adv.* **2011**, *1*, 1772–1777.
- (15) Tang, Z. R.; Li, F.; Zhang, Y.; Fu, X.; Xu, Y. J. *J. Phys. Chem. C* **2011**, *115*, 7880–7886.
- (16) Bavykin, D. V.; Walsh, F. C. *Eur. J. Inorg. Chem.* **2009**, 977–997.
- (17) Zhang, Y.; Tang, Z. R.; Fu, X.; Xu, Y. J. *ACS Nano* **2010**, *4*, 7303–7314.
- (18) Zhang, N.; Liu, S.; Fu, X.; Xu, Y. J. *J. Phys. Chem. C* **2011**, *115*, 9136–9145.
- (19) Xu, Y. J.; Zhuang, Y.; Fu, X. J. *J. Phys. Chem. C* **2010**, *114*, 2669–2676.
- (20) Zhang, Y.; Tang, Z. R.; Fu, X.; Xu, Y. J. *Appl. Catal., B* **2011**, *106*, 445–452.
- (21) Khan, S. U. M.; Al-Shahry, M.; Ingler, W. B. Jr. *Science* **2002**, *297*, 2243–2245.
- (22) Zhang, Y.; Tang, Z. R.; Fu, X.; Xu, Y. J. *ACS Nano* **2011**, *5*, 7426–7435.
- (23) Ma, R.; Bando, Y.; Sasaki, T. *Chem. Phys. Lett.* **2003**, *380*, 577–582.
- (24) Nakahira, A.; Kubo, T.; Numako, C. *Inorg. Chem.* **2010**, *49*, 5845–5852.
- (25) Ma, R.; Fukuda, K.; Sasaki, T.; Osada, M.; Bando, Y. *J. Phys. Chem. B* **2005**, *109*, 6210–6214.
- (26) Liu, P.; Zhang, H.; Liu, H.; Wang, Y.; Yao, X.; Zhu, G.; Zhang, S.; Zhao, H. *J. Am. Chem. Soc.* **2011**, *133*, 19032–19035.
- (27) Jennings, J. R.; Ghicov, A.; Peter, L. M.; Schmuiki, P.; Walker, A. B. *J. Am. Chem. Soc.* **2008**, *130*, 13364–13372.
- (28) Zhu, K.; Neale, N. R.; Miedaner, A.; Frank, A. J. *Nano Lett.* **2007**, *7*, 69–74.
- (29) Liu, S. M.; Gan, L. M.; Liu, L. H.; Zhang, W. D.; Zeng, H. C. *Chem. Mater.* **2002**, *14*, 1391–1397.
- (30) Hoyer, P. *Langmuir* **1996**, *12*, 1411–1413.
- (31) Bae, C.; Yoo, H.; Kim, S.; Lee, K.; Kim, J.; Sung, M. M.; Shin, H. *Chem. Mater.* **2008**, *20*, 756–767.
- (32) Yu, J.; Dai, G.; Cheng, P. *J. Phys. Chem. C* **2010**, *114*, 19378–19385.
- (33) Liao, Y.; Que, W.; Zhong, P.; Zhang, J.; He, Y. *ACS Appl. Mater. Interfaces* **2011**, *3*, 2800–2804.
- (34) Du, G. H.; Chen, Q.; Che, R. C.; Yuan, Z. Y.; Peng, L. M. *Appl. Phys. Lett.* **2001**, *79*, 3702–3704.
- (35) Tian, Z. R.; Voigt, J. A.; Liu, J.; McKenzie, B.; Xu, H. *J. Am. Chem. Soc.* **2003**, *125*, 12384–12385.
- (36) Kasuga, T.; Hiramatsu, M.; Hoson, A.; Sekino, T.; Niihara, K. *Langmuir* **1998**, *14*, 3160–3163.
- (37) Tsai, C. C.; Teng, H. *Chem. Mater.* **2004**, *16*, 4352–4358.
- (38) Sun, X.; Li, Y. *Chem.—Eur. J.* **2003**, *9*, 2229–2238.
- (39) Kiatkittipong, K.; Scott, J.; Amal, R. *ACS Appl. Mater. Interfaces* **2011**, *3*, 3988–3996.
- (40) Yu, J.; Yu, H.; Cheng, B.; Trapalis, C. *J. Mol. Catal., A* **2006**, *249*, 135–142.
- (41) Qamar, M.; Yoon, C. R.; Oh, H. J.; Lee, N. H.; Park, K.; Kim, D. H.; Lee, K. S.; Lee, W. J.; Kim, S. J. *Cat. Today* **2008**, *131*, 3–14.
- (42) Ou, H. H.; Liao, C. H.; Liou, Y. H.; Hong, J. H.; Lo, S. L. *Environ. Sci. Technol.* **2008**, *42*, 4507–4512.
- (43) Zhang, H.; Li, G. R.; An, L. P.; Yan, T. Y.; Gao, X. P.; Zhu, H. Y. *J. Phys. Chem. C* **2007**, *111*, 6143–6148.
- (44) Li, J.; Tang, Z.; Zhang, Z. *Chem. Phys. Lett.* **2006**, *418*, 506–510.
- (45) Bavykin, D. V.; Walsh, F. C. *Titanate and Titania Nanotubes: Synthesis, Properties and Applications (RSC Nanoscience and Nanotechnology)*; RSC Publishing: Cambridge, U.K., 2010.
- (46) Li, J.; Tang, Z.; Zhang, Z. *Electrochem. Commun.* **2005**, *7*, 62–67.
- (47) Zhu, K.; Vinzant, T. B.; Neale, N. R.; Frank, A. J. *Nano Lett.* **2007**, *7*, 3739–3746.
- (48) Shankar, K.; Basham, J. I.; Allam, N. K.; Varghese, O. K.; Mor, G. K.; Feng, X.; Paulose, M.; Seabold, J. A.; Choi, K. S.; Grimes, C. A. *J. Phys. Chem. C* **2009**, *113*, 6327–6359.
- (49) Ohsaki, Y.; Masaki, N.; Kitamura, T.; Wada, Y.; Okamoto, T.; Sekino, T.; Niihara, K.; Yanagida, S. *Phys. Chem. Chem. Phys.* **2005**, *7*, 4157–4163.
- (50) Thorne, A.; Kruth, A.; Tunstall, D.; Irvine, J. T. S.; Zhou, W. *J. Phys. Chem. B* **2005**, *109*, 5439–5444.
- (51) Chatterjee, S.; Bhattacharyya, K.; Arrub, P.; Tyagi, A. K. *J. Phys. Chem. C* **2010**, *114*, 9424–9430.
- (52) Lee, C. K.; Wang, C. C.; Lyn, M. D.; Juang, L. C.; Liu, S. S.; Hung, S. H. *J. Colloid Interface Sci.* **2007**, *316*, 562–569.
- (53) Grandcolas, M.; Louvet, A.; Keller, N.; Keller, V. *Angew. Chem., Int. Ed.* **2008**, *121*, 167–170.
- (54) Gao, T.; Norby, P.; Okamoto, H.; Fjellva' g, H. *Inorg. Chem.* **2009**, *48*, 9409–9418.
- (55) Wang, M.; Song, G.; Li, J.; Miao, L.; Zhang, B. *J. Univ. Sci. Technol. Beijing* **2008**, *15*, 644–648.
- (56) Zhang, N.; Zhang, Y. H.; Pan, X. Y.; Fu, X.; Xu, Y. J. *Sci. China Chem.* **2011**, *41*, 1097–1111.
- (57) Zhang, N.; Fu, X.; Xu, Y. J. *J. Mater. Chem.* **2011**, *21*, 8152–8158.

- (58) Zhang, N.; Zhang, Y.; Pan, X.; Fu, X.; Liu, S.; Xu, Y. *J. Phys. Chem. C* **2011**, *115*, 23501–25311.
- (59) Zhang, N.; Liu, S.; Fu, X.; Xu, Y. *J. Phys. Chem. C* **2011**, *115*, 22901–22909.
- (60) Maldotti, A.; Molinari, A.; Amadelli, R. *Chem. Rev.* **2002**, *102*, 3811–3836.
- (61) Yang, P.; Song, C.; Lv, M.; Zhou, G.; Yang, Z.; Xu, D.; Yuan, D. *J. Phys. Chem. Solids* **2002**, *63*, 639–643.
- (62) Wu, Y.; Lu, G.; Li, S. *J. Photochem. Photobiol., A* **2006**, *181*, 263–267.
- (63) Su, H.; Li, J.; Tan, T. *Biochem. Eng. J.* **2008**, *39*, 503–509.
- (64) Graat, P. C. J.; Somers, M. A. J. *Appl. Surf. Sci.* **1996**, *100*, 36–40.
- (65) Akhtar, A. S.; Wong, K. C.; Wong, P. C.; Mitchell, K. A. R. *Thin Solid Films* **2007**, *515*, 7899–7905.